CONTRIBUTION OF FIN TO SIDEFORCE, YAWING MOMENT AND ROLLING MOMENT DERIVATIVES DUE TO SIDESLIP, $(Y_v)_F$, $(N_v)_F$, $(L_v)_F$, IN THE PRESENCE OF BODY, WING AND TAILPLANE

1. NOTATION AND UNITS (see Sketches 1.1, 1.2 and 1.3)

The derivative notation used is that proposed in ARC R&M 3562 (Hopkin, 1970) and described in Item No. 86021. Coefficients and aeronormalised derivatives are evaluated in aerodynamic body axes with origin at the aircraft centre of gravity and with the wing span as the characteristic length. The derivatives Y_v, N_v and L_v are often written as $\partial C_Y/\partial\beta$, $\partial C_n/\partial\beta$ and $\partial C_l/\partial\beta$ or $C_{Y\beta}$, $C_{n\beta}$ and $C_{l\beta}$ in other systems of notation, but attention must be paid to the reference dimensions used and it is to be noted that a constant datum value of V is employed in the Hopkin system.

		SI	*British*
A_W	wing aspect ratio, b^2/S_W		
A_F	effective aspect ratio of fin, $2h_F^2/S_F$, see Section 3.2		
A_T	tailplane aspect ratio, b_T^2/S_T		
b	wing span	m	ft
b_T	tailplane span	m	ft
$(C_{L\alpha})_F$	lift-curve slope, $\partial C_L/\partial\alpha$, for straight-tapered wing of aspect ratio A_F, taper ratio λ_F, half-chord sweep angle $\Lambda_{½F}$ and area $2S_F$, estimated from Item No. 70011 (Derivation 33), see Section 3.2	radian^{-1}	radian^{-1}
C_l	rolling moment coefficient, $\mathscr{L}/½\rho V^2 S_W b$		
C_n	yawing moment coefficient, $\mathscr{N}/½\rho V^2 S_W b$		
C_Y	sideforce coefficient, $Y/½\rho V^2 S_W$		
c_{0T}	tailplane centre-line chord, in plane of symmetry through body centre-line	m	ft
c_{rF}	fin root chord, see Section 3.2	m	ft
c_{tF}	fin tip chord, see Section 3.2	m	ft
c_{tT}	tailplane tip chord	m	ft
d_{BF}	body width at fin root quarter-chord station	m	ft
h_{BF}	body height at fin root quarter-chord station	m	ft

h_{BW}	body height at wing root quarter-chord station, see Sketch 1.1	m	ft
h_F	height of fin, measured from fin root chord in direction normal to longitudinal body axis see Section 3.2	m	ft
J_B	sideforce correction factor allowing for presence of body		
J_T	sideforce correction factor allowing for presence of tailplane		
J_W	sideforce correction factor allowing for presence of wing		
$\mathscr{L}$	rolling moment	N m	lbf ft
L_v	rolling moment derivative due to sideslip, $L_v = (\partial\mathscr{L}/\partial v)/½\rho V S_W b$		
$(L_v)_F$	fin contribution to L_v in presence of body, wing and tailplane		
M	free-stream Mach number		
m_F	distance of fin root quarter-chord station aft of centre of gravity position (moment reference centre), measured parallel to aircraft longitudinal body axis	m	ft
$\mathscr{N}$	yawing moment	N m	lbf ft
N_v	yawing moment derivative due to sideslip, $N_v = (\partial\mathscr{N}/\partial v)/½\rho V S_W b$		
$(N_v)_F$	fin contribution to N_v in presence of body, wing and tailplane		
S_F	fin area, $h_F(c_{rF}+c_{tF})/2$, see Section 3.2	m^2	ft^2
S_T	tailplane area, $b_T(c_{0T}+c_{tT})/2$	m^2	ft^2
S_W	wing (reference) area	m^2	ft^2
V	velocity of aircraft relative to air	m/s	ft/s
v	sideslip velocity	m/s	ft/s
Y	sideforce	N	lbf
Y_v	sideforce derivative, $Y_v = (\partial Y/\partial v)/½\rho V S_W$		
$(Y_v)_F$	fin contribution to Y_v in presence of body, wing and tailplane		
z_{crF}	height of fin root chord, measured from longitudinal body axis in direction normal to longitudinal body axis	m	ft

$\overline{z}_F$	height of centre of pressure position of load distribution on fin, measured from fin root chord in direction normal to longitudinal body axis, see Section 3.6	m	ft
z_T	height of intersection of fin-mounted tailplane with fin, measured from fin root chord in direction normal to longitudinal body axis	m	ft
z_W	height of wing root quarter-chord point above local body centre-line, positive for low wings, see Sketch 1.1	m	ft
α	angle of attack	radian	radian
β	angle of sideslip	radian	radian
$\Lambda_{¼F}$	fin quarter-chord sweep angle	degree	degree
$\Lambda_{½F}$	fin half-chord sweep angle	degree	degree
$\Lambda_{¼T}$	tailplane quarter-chord sweep angle	degree	degree
$\Lambda_{¼W}$	wing quarter-chord sweep angle	degree	degree
λ_F	ratio c_{tF}/c_{rF}		
λ_T	ratio c_{tT}/c_{0T}		
ρ	density of air	kg/m^3	$slug/ft^3$

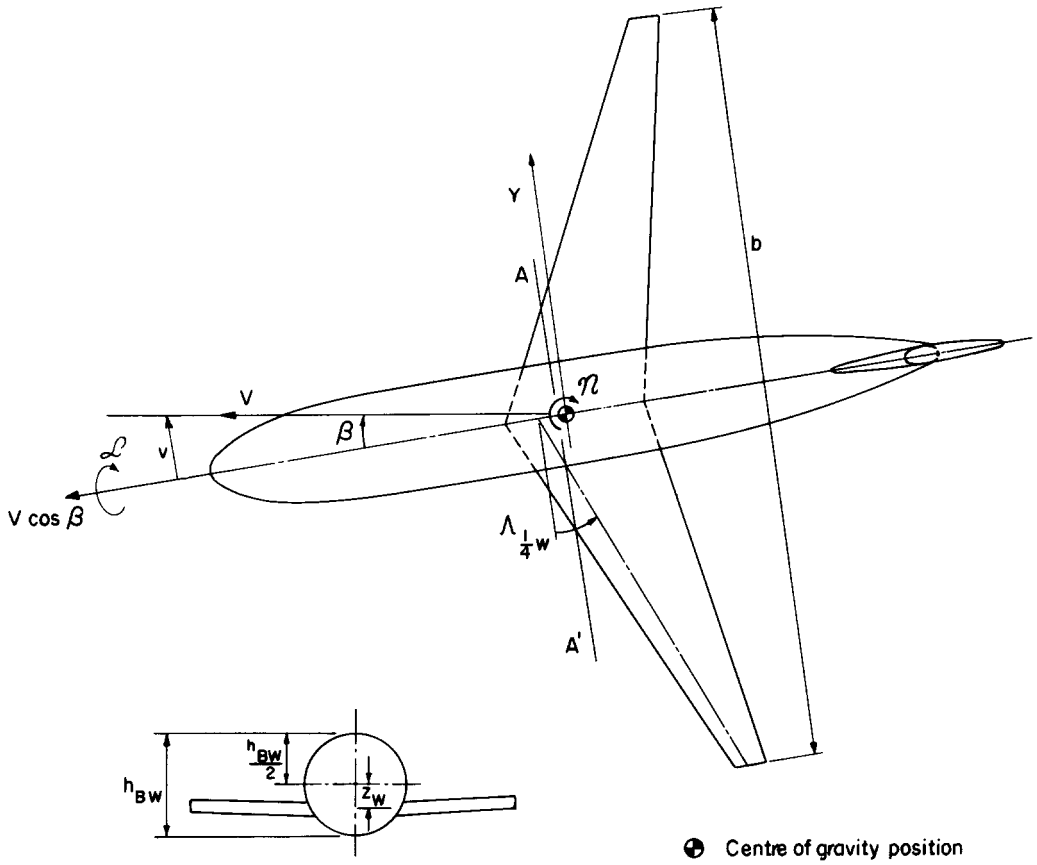

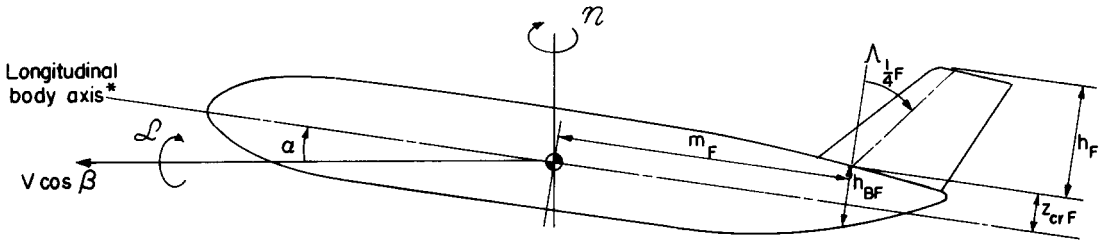

Sketch 1.1 Body, wing and fin geometries

* The longitudinal body axis is a reference axis, fixed in the body in the plane of symmetry and passing through the centre of gravity position. The exact direction of the axis in the plane of symmetry is conventionally determined by considerations of mid-body geometry, the axis being taken parallel to some convenient "horizontal" datum.

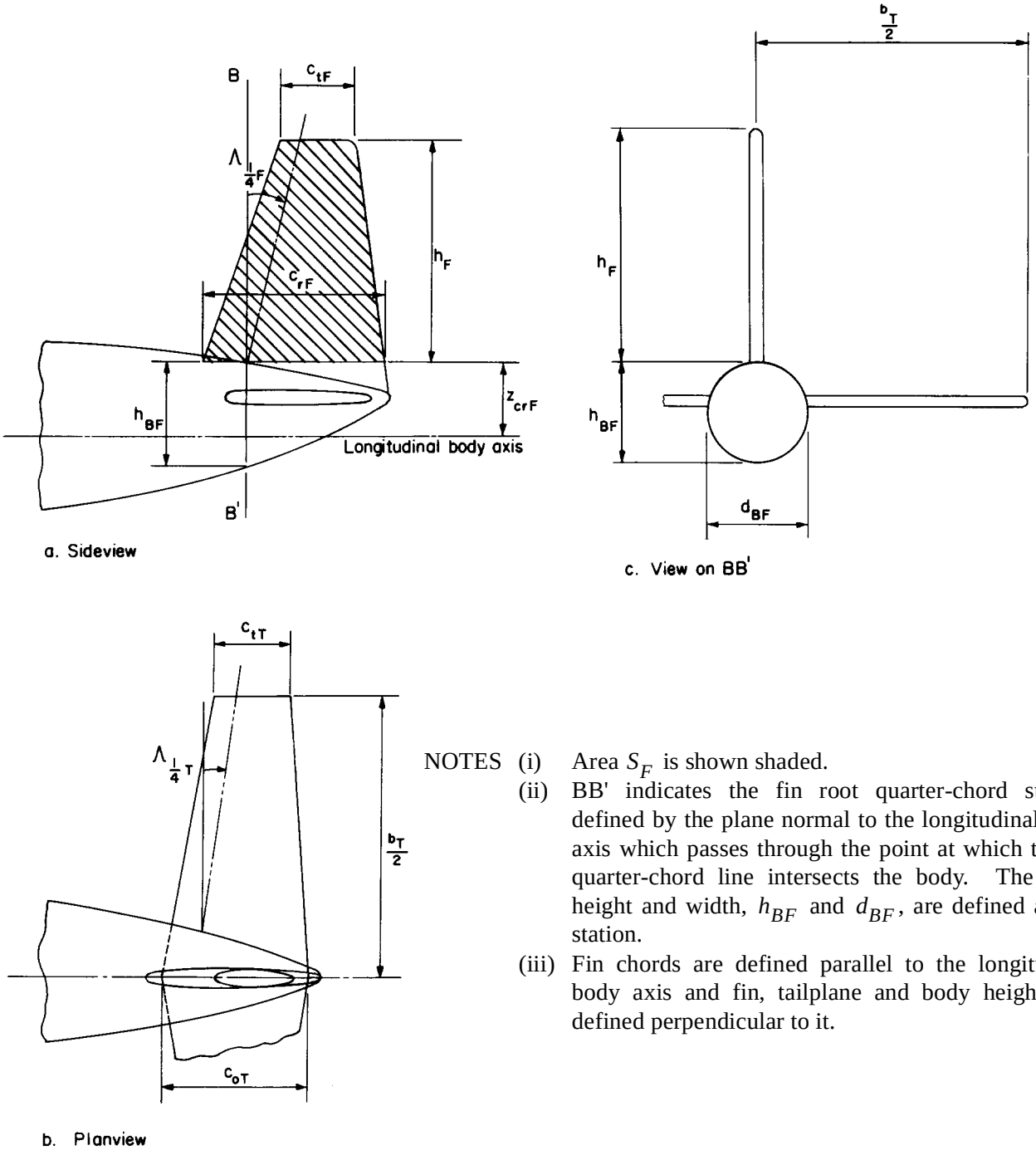

NOTES (i) Area S_F is shown shaded.

(ii) BB' indicates the fin root quarter-chord station, defined by the plane normal to the longitudinal body axis which passes through the point at which the fin quarter-chord line intersects the body. The body height and width, h_{BF} and d_{BF}, are defined at this station.

(iii) Fin chords are defined parallel to the longitudinal body axis and fin, tailplane and body heights are defined perpendicular to it.

Sketch 1.2 Fin and tailplane geometries for body-mounted tailplanes

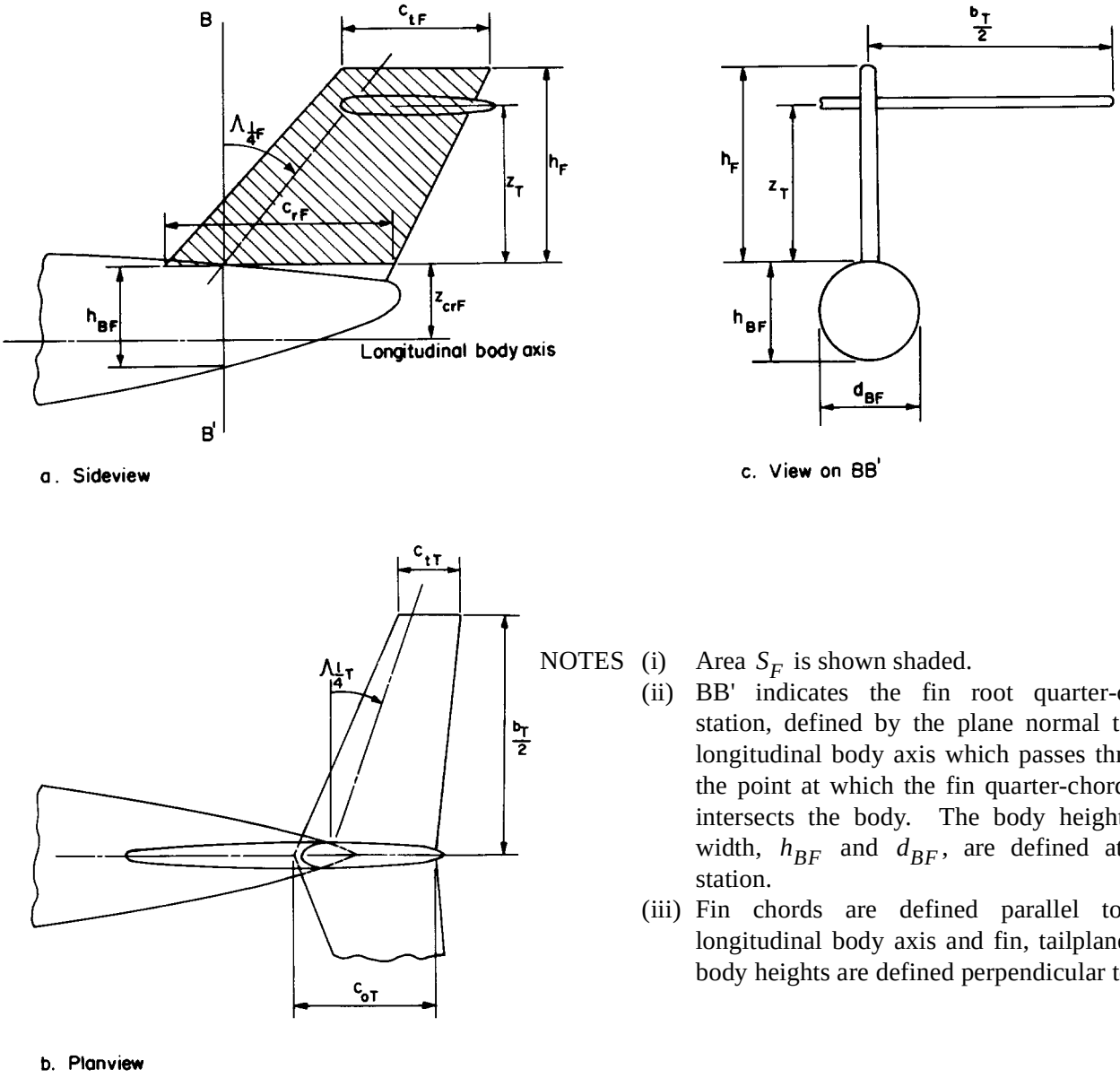

NOTES (i) Area S_F is shown shaded.

(ii) BB' indicates the fin root quarter-chord station, defined by the plane normal to the longitudinal body axis which passes through the point at which the fin quarter-chord line intersects the body. The body height and width, h_{BF} and d_{BF}, are defined at this station.

(iii) Fin chords are defined parallel to the longitudinal body axis and fin, tailplane and body heights are defined perpendicular to it.

Sketch 1.3 Fin and tailplane geometries for fin-mounted tailplanes

2. INTRODUCTION

This Item gives a semi-empirical method for calculating $(Y_v)_F$, $(N_v)_F$, and $(L_v)_F$, the contributions of the vertical stabilising fin of an aircraft to the sideforce, yawing moment and rolling moment derivatives due to sideslip, at subsonic speeds. The aircraft geometries covered by the method are those where a single fin is located on top of the aircraft rear-body, and in the plane of symmetry, with the tailplane mounted either on the fin itself or on the rear-body. The shape of the fin is assumed to approximate to a trapezium. The method was developed for bodies with circular or nearly-circular cross-sections. It may be used, with caution, for bodies with elliptical or near-rectangular cross-sections by using a mean body diameter provided that the body height to width ratio in the region of the fin is close to unity. Otherwise the method of Item No. 93007 (Reference 39) that covers a wide range of body height to width ratios and both single and twin fins should be used.

The method was established on the basis of a large number of comparisons with the wind-tunnel data in Derivations 1 to 31, with the theoretical method given in Derivation 32 being used to provide some guidance on the effect of systematic variations of body, fin and tailplane geometries in areas where the experimental data were sparse or highly scattered. (Derivation 32 uses a potential-flow calculation to determine the side-load distribution over body-fin-tailplane assemblies, see Section 2.1.)

The predicted contributions $(Y_v)_F$, $(N_v)_F$ and $(L_v)_F$ include allowances for interference between the body, wing, tailplane and fin and represent the effect of adding a fin. In particular the additional load induced on the body by the fin is taken into account. To estimate the total values of the stability derivatives for an aircraft the predicted contributions from the wing, body, nacelles and trailing-edge flaps must be added to the fin contributions predicted herein, as described in Item No. 82011 (Reference 38) for Y_v and N_v and Item No. 81032 (Reference 37) for L_v.*

The method is described in detail in Section 3. The accuracy and applicability, including comments on body cross-section shape and dorsal fin extensions, are discussed in Section 4. The Derivation and References are given in Section 5, and a worked example is given in Section 6.

2.1 Note on Method in Derivation 32

In Derivation 32 the sideforce distributions on body-fin-tailplane assemblies are calculated for configurations where there is constant induced sidewash across the fin span. The distributions are calculated from the two-dimensional flow around the cross-section of the wake in the Trefftz-plane, with conformal mappings being used to transform this flow into the flow past a flat plate, for which the potential flow function is known. The local difference of the potential flow function to either side of the flat plate gives the sideforce distributions.

The assumption of constant induced sidewash imposes a restriction on the planforms of the fin and the tailplane, the twist of the tailplane and the shape of the body. As the aspect ratios of the tailplane and fin become very small the condition of constant induced sidewash is satisfied whatever the shape of the fin and tailplane, provided that they are plane surfaces, that the twist of the tailplane tends to zero and that the body tends to a cylindrical cross-section. The calculation is therefore exact in the limiting case of very small fins and tailplanes and differences between any given arrangement and the constant induced sidewash arrangement appear only when the aspect ratio is not small. However, Derivation 32 suggests that at least approximate calculations can be made even for arrangements of large aspect ratio when the differences between a given arrangement and the constant induced sidewash arrangement can be expected to be appreciable. The method was therefore considered suitable for use in this Item to obtain smooth variations through scattered data and to provide guidance in areas where there were few data, provided experimental data were used as a check on magnitudes.

* Contributions from the tailplane in addition to the interference effects considered in this Item are discussed in Item No. 82011 (Section 3.2.2) and Item No. 81032. They are generally small enough to be neglected. If the tailplane has a large dihedral angle Item No. 81032 describes how the small tailplane-dihedral component of L_v can be calculated using the isolated wing data in Item No. Aero A.06.01.03 (Reference 35).

3. METHOD

3.1 General Description

3.1.1 Sideforce derivative $(Y_v)_F$

The derivative $(Y_v)_F$ is calculated by applying a series of correction factors to a basic lift-curve slope, $(C_{L\alpha})_F$, estimated for the fin. The correction factors allow, separately, for the presence of the body, tailplane and wing and are denoted by J_B, J_T and J_W respectively. The derivative $(Y_v)_F$ is given by

$$(Y_v)_F = -J_B J_T J_W (C_{L\alpha})_F S_F / S_W . \tag{3.1}$$

The establishment of the fin geometry and the calculation of $(C_{L\alpha})_F$ are described in Section 3.2, and the interference factors J_B, J_T and J_W are described in Sections 3.3 to 3.5, respectively.

3.1.2 Yawing moment and rolling moment derivatives $(N_v)_F$ and $(L_v)_F$

The derivatives $(N_v)_F$ and $(L_v)_F$ are calculated by estimating an approximate centre of pressure position for the sideforce generating $(Y_v)_F$ and thence determining the yawing and rolling moments produced relative to the centre of gravity position. Section 3.6 describes how the centre of pressure position is calculated by initially considering a simple spanwise loading distribution over the fin and then applying two numerical constants to modify the vertical and longitudinal moment arms in order to improve the accuracy of prediction of $(N_v)_F$ and $(L_v)_F$. The effect of the numerical constants is to allow empirically for the division of the sideforce between the fin and the body. The centre of pressure position of the fin loading is expressed in terms of its height $\bar{z}_F$ perpendicularly above the fin root chord and its longitudinal distance $\bar{z}_F \tan\Lambda_{¼F}$ aft of the fin root quarter-chord station. The numerical constants modify these distances to $0.85\bar{z}_F$ and $0.7\bar{z}_F \tan\Lambda_{¼F}$. Relative to the centre of gravity position the moment arms of the sideforce in directions perpendicular and parallel to the longitudinal body axis become $z_{crF} + 0.85\bar{z}_F$ and $m_F + 0.7\bar{z}_F \tan\Lambda_{¼F}$ respectively. In the aerodynamic body axis system the yawing and rolling moment derivatives are therefore

$$(N_v)_F = -(Y_v)_F[(m_F + 0.7\bar{z}_F \tan\Lambda_{¼F})\cos\alpha + (z_{crF} + 0.85\bar{z}_F)\sin\alpha]/b \tag{3.2}$$

and

$$(L_v)_F = (Y_v)_F[(z_{crF} + 0.85\bar{z}_F)\cos\alpha - (m_F + 0.7\bar{z}_F \tan\Lambda_{¼F})\sin\alpha]/b . \tag{3.3}$$

At low values of α, since the resolved component of the longitudinal moment arm is usually much greater than the resolved component of the vertical moment arm, $(N_v)_F$ can normally be approximated by

$$(N_v)_F = -(Y_v)_F(m_F + 0.7\bar{z}_F \tan\Lambda_{¼F})/b . \tag{3.4}$$

No such simplification is possible in the case of $(L_v)_F$ since the resolved components of the moment arms are of comparable magnitudes.

3.2 Fin Geometry and Lift-curve Slope

To calculate the basic lift-curve slope of the fin, $(C_{L\alpha})_F$, the actual fin is represented as a trapezoidal panel. This is then considered to form half of a straight-tapered wing for which a lift-curve slope can be evaluated from Item No. 70011 (Derivation 33).

The trapezoidal panel is defined by the leading and trailing edges, the tip chord and the root chord of the fin. Sketches 1.2 and 1.3 show the trapezoidal panel shaded. Note that the fin chords and heights are defined parallel and perpendicular to the longitudinal body axis. Any extension to the fin leading-edge in the vicinity of the body junction by means of a dorsal fairing* and any curvature of the fin tip are ignored by extending the fin leading-edge linearly into the body and to the maximum fin height, as shown in Sketch 3.1. The fin panel tip chord, c_{tF}, is the chordwise distance between the leading and trailing edges of the fin at the maximum height. The fin panel root chord, c_{rF}, is the chordwise distance between the (extrapolated) leading and trailing edges of the fin at the height where the fin quarter-chord sweep line intersects the top of the body. The plane normal to the longitudinal body axis and passing through this point of intersection defines the fin root quarter-chord station, The fin height, h_F, is the perpendicular distance between the fin root and tip chords. The fin area, S_F, is the area enclosed by the fin (linear) leading and trailing edges, the fin tip chord and the fin root chord, so that

$$S_F = h_F(c_{rF} + c_{tF})/2\,. \tag{3.5}$$

The straight-tapered wing is formed by reflecting the trapezoidal panel about its root chord. This wing has an aspect ratio

$$A_F = 2h_F^2/S_F, \tag{3.6}$$

a taper ratio

$$\lambda_F = c_{tF}/c_{rF}, \tag{3.7}$$

and a half-chord sweep angle parameter defined by the equation

$$A_F \tan\Lambda_{½F} = A_F \tan\Lambda_{¼F} - \left(\frac{1-\lambda_F}{1+\lambda_F}\right). \tag{3.8}$$

The lift-curve slope predicted for such a wing by Item No. 70011, and based on the area $2S_F$, is used as the basic lift-curve slope of the fin $(C_{L\alpha})_F$. Equation (3.1) corrects to the half-wing area S_F appropriate to the fin. The data in Item No. 70011 allow for compressibility effects and $(C_{L\alpha})_F$ should be calculated for the free-stream Mach number of interest.

* The effect of dorsal fairings on the stability derivatives is discussed in Section 4.2.3.

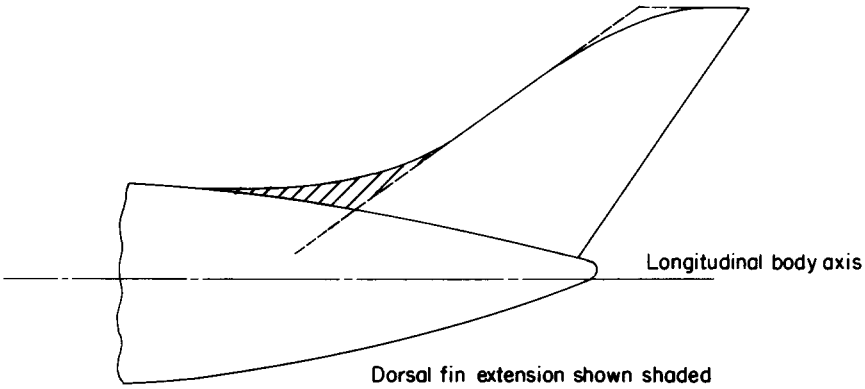

Sketch 3.1 Definition of fin leading edge

3.3 Body-fin Correction Factor

The correction factor J_B allows for the effect of the body on the basic fin lift-curve slope and is given in Figure 1. It is presented as a function of $h_{BF}/(h_{BF}+h_F)$ and A_F, where h_{BF} is the body height at the fin root quarter-chord station and h_F is the fin height. It was obtained by comparing experimental values of $(Y_v)_F$ for body-fin combinations with the values of $(C_{L\alpha})_F$ calculated as described in Section 3.2. There was good agreement between the theoretical values of J_B predicted by the method in Derivation 32 and the values deduced from the experimental data, although the latter were subject to significant scatter. Therefore, smooth variations through the experimental data were obtained by following the predicted trends with $h_{BF}/(h_{BF}+h_F)$ and A_F and applying empirical corrections in magnitude to improve the overall accuracy.

3.4 Tailplane Correction Factor

The correction factor J_T allows for the interference effect of a tailplane on the sideforce derivative. It is given in Figure 2a for body-mounted tailplanes and in Figure 2b for fin-mounted tailplanes. Figure 2a presents J_T as a function of $h_{BF}/(h_{BF}+h_F)$ and b_T/h_F, where b_T is the tailplane span. Figure 2b presents J_T as a function of b_T/h_F and z_T/h_F, where z_T is the height of the intersection of the tailplane with the fin, measured from the fin root chord. The Figures were developed by comparing experimental values of $(Y_v)_F$ for configurations tested both with and without a tailplane. Most of the data studied were for tailplanes with spans in the range $2 \le b_T/h_F \le 4$, which enabled the curves in Figures 2a and 2b to be established for tailplanes of this size. Comparisons with the values of J_T predicted by the method of Derivation 32 were used to obtain a smooth variation with b_T/h_F and, in Figure 2a, with $h_{BF}/(h_{BF}+h_F)$. Only a few experimental data were available for tailplane spans with $b_T/h_F = 1$ and 0.5 but these confirmed the trends predicted. The curves at $b_T/h_F = 0.25$ should be regarded as tentative and are included to provide a smooth variation into $J_T = 1$.

For body-mounted tailplanes the theoretical calculations and the experimental data from which values of J_T could be obtained were limited to configurations with tailplanes mounted on or near the local body centre-line. Some caution is therefore necessary when using the method for tailplanes mounted high on the body close to the fin-body junction. However, in the absence of other information, the values of J_T given in Figure 2a should be employed for all body-mounted tailplanes. For fin-mounted tailplanes the height of the tailplane is assumed to lie in the range $0.25 \le z_T/h_F \le 1$, which covers most practical arrangements.

3.5 Wing Correction Factor

The correction factor J_W allows for interference between the wing and the body-fin-tailplane assembly. It is given in Figure 3a for configurations with body-mounted tailplanes and in Figure 3b for configurations where the tailplane is fin-mounted or absent. In both cases J_W is a function of the wing height, expressed as z_W/h_{BW}, the ratio of the distance of the wing root quarter-chord point from the local body centre-line to the body height at the wing root quarter-chord station, see Sketch 1.1.

There was no theoretical method available for predicting J_W and Figures 3a and 3b were produced solely from an examination of the experimental data in Derivations 1 to 31. A small number of data (Derivations 2, 3, 5, 11 and 14) were available in which a configuration was tested with a wing in a high, a middle and a low position, other parameters remaining constant. Comparing the values of $(Y_v)_F$ for the high- and low-wing configurations with the value for the corresponding mid-wing configuration enabled estimates of J_W to be made for values of $|z_W/h_{BW}|$ between 0.35 and 0.40. Efforts were made to establish the variation of J_W at other values of z_W/h_{BW} by comparing the experimental values of $(Y_v)_F$ for complete models with the predictions resulting from Equation (3.1) with $J_W = 1$. These confirmed the general trends apparent from the systematic tests and the curves shown are mean values drawn through the experimental data. The general scatter of the data defining the J_W curves was about ± 0.1, and in one or two cases comparisons with the data for complete models suggested larger departures. There were no data for wings displaced only slightly from the mid-wing position and the shapes of the curves in the regions $-0.3 \le z_W/h_{BW} \le 0.1$ in Figure 3a and $-0.2 \le z_W/h_{BW} \le 0.2$ in Figure 3b are based on interpolation between the experimental data and the mid-wing value of unity. Some caution is therefore necessary when taking values of J_W from Figures 3a and 3b. In particular, undue reliance should not be placed on the predicted benefit in fin effectiveness to be gained from wings mounted low on the body.

3.6 Centre of Pressure Position

The centre of pressure position calculated in this Section is intended only as a suitable representation of the point of action of the fin sideforce for the purposes of calculating $(N_v)_F$ and $(L_v)_F$. It has been obtained by first calculating a position based on simple assumptions concerning the loading on the fin and then applying two numerical correction factors to the vertical and longitudinal positions in order to improve the overall agreement between the predicted and experimental values of $(N_v)_F$ and $(L_v)_F$. The scatter between the experimental and predicted values of $(Y_v)_F$ is too great (see Section 4.1) to warrant a more elaborate treatment since it would lead to little improvement in accuracy.

The centre of pressure position associated with the loading on the fin is expressed in terms of its height perpendicularly above the fin root chord, $\bar{z}_F$, and its longitudinal distance aft of the fin root quarter-chord station, $\bar{z}_F \tan \Lambda_{¼F}$, the sideforce being assumed to act on the fin quarter-chord line. For body-mounted tailplanes, or when the tailplane is absent, a half-wing elliptical spanwise loading over the fin is assumed, and this gives a vertical centre of pressure position at approximately 40 per cent of the fin height, *i.e.* at a distance $0.4h_F$ above the fin root chord. When the tailplane is mounted on the fin the parts of the sideforce acting on the fin above and below the tailplane are considered separately, and a half-wing elliptical spanwise loading is assumed over the fin extent to either side of the tailplane. This gives a centre of pressure position for each part of the sideforce which is at approximately 40 per cent of the fin extent to either side of the tailplane. Therefore the fin load above the tailplane acts at a distance $z_T + 0.4(h_F - z_T)$ above the fin root chord, and the fin load below the tailplane acts at a distance $0.6z_T$ above the fin root chord. The overall centre of pressure position is obtained by assuming that the magnitudes of the loads above and below the tailplane are in the same ratio as the fin areas above and below the tailplane, and by taking moments about the fin root chord. Figure 4 shows the result of this calculation for a fin with $\lambda_F = 0.6$, presenting $\bar{z}_F/h_F$ as a function of z_T/h_F. Comparisons with a large number of experimental data covering fin taper ratios in the range $0.25 \le \lambda_F \le 1$ have shown that the variation of $\bar{z}_F$ with tailplane height given in Figure 4 can be used for any taper ratio in this range with no loss of accuracy. This is because any change due to varying

the taper ratio can have only a small effect on the overall moment arms relative to the centre of gravity position, particularly in the case of $(N_v)_F$.

Examination of the experimental data in Derivations 1 to 31 and the values predicted for $(N_v)_F$ and $(L_v)_F$ on the basis of the vertical and longitudinal moment arms $\bar{z}_F$ and $\bar{z}_F \tan\Lambda_{¼}$, corrected to the centre of gravity position, showed that the magnitudes of $(N_v)_F$ and $(L_v)_F$ were slightly overestimated in general and that improved predictions were obtained if two numerical constants were introduced to reduce the moment arms. These constants may be considered as empirical corrections to allow for the fact that part of the sideforce is carried on the body and acts below the fin root chord, with a point of action which is near to the fin root quarter-chord station and not on the fin quarter-chord line. Relative to the centre of gravity position the modified moment arms are $z_{crF} + 0.85\bar{z}_F$ and $m_F + 0.7\bar{z}_F \tan\Lambda_{¼F}$ (with $\bar{z}_F$ taken from Figure 4). Although they are based on a simple treatment of the body-fin-tailplane loading, comparisons with experimental data for a wide range of configurations have shown that these arms provide a suitable basis for calculations of lateral stability. Equations (3.2) and (3.3) in Section 3.1.2 show how they are combined with $(Y_v)_F$ and the angle of attack α for predicting $(N_v)_F$ and $(L_v)_F$ in the aerodynamic body axis system.

4. ACCURACY AND APPLICABILITY

4.1 Accuracy

Sketches 4.1 to 4.3 illustrate the general level of agreement between the predicted and experimental values of $(Y_v)_F$, $(N_v)_F$ and $(L_v)_F$. The values of $(Y_v)_F$ are generally predicted to within ± 0.08 and the values of $(N_v)_F$ to within ± 0.04. There is relatively greater scatter between the predicted and experimental values of $(L_v)_F$. This is partly due to the fact that the experimental values of L_v are sometimes less easy to define in terms of an idealised linear variation of rolling moment with angle of sideslip than is the case when defining Y_v and N_v from sideforce and yawing moment data. It also reflects the fact that because of the smaller magnitude of L_v and its greater dependence on angle of attack the identification of the fin contribution from experimental data is subject to higher errors. Overall the values of $(L_v)_F$ are generally predicted to within ± 0.02.

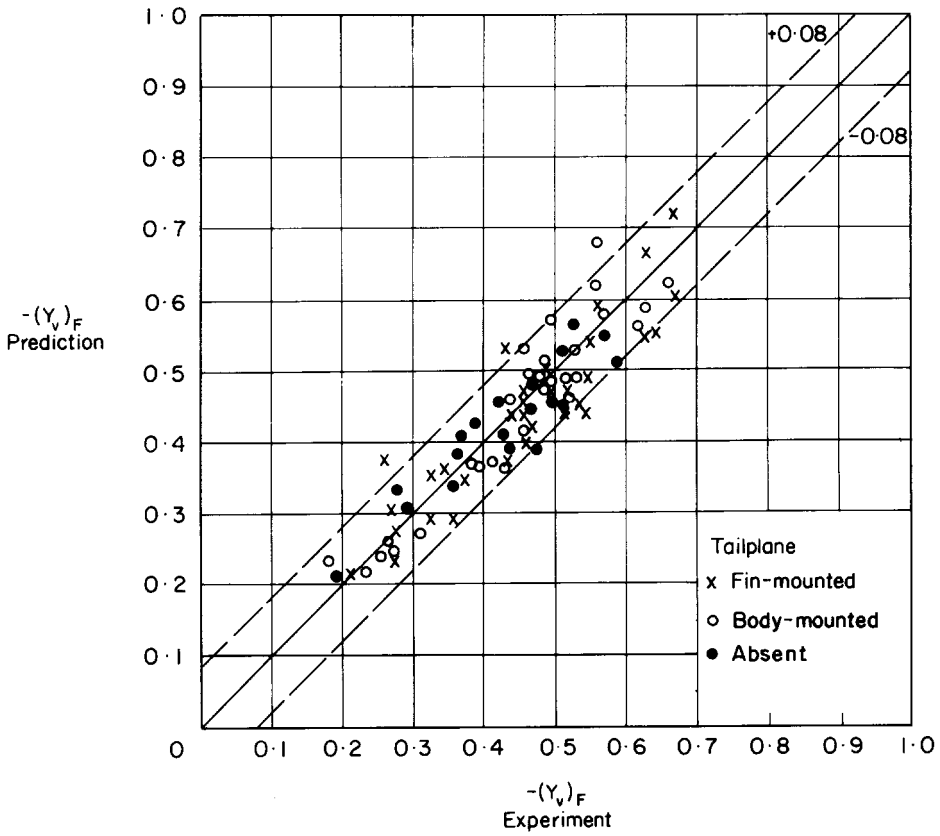

Sketch 4.1

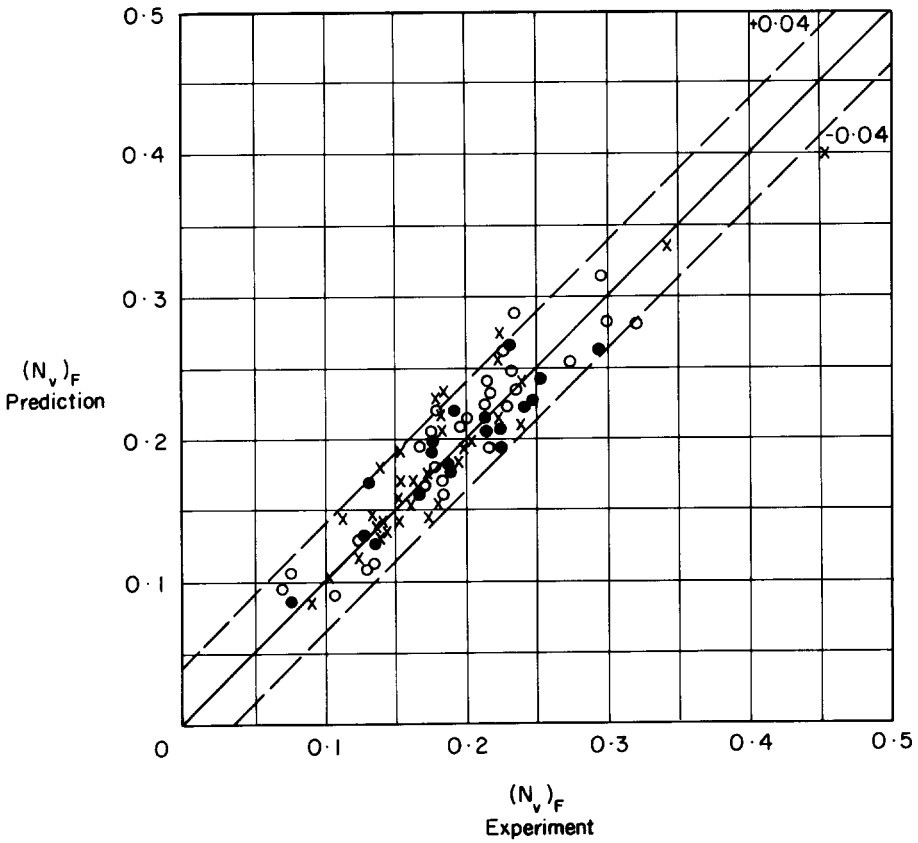

Sketch 4.2

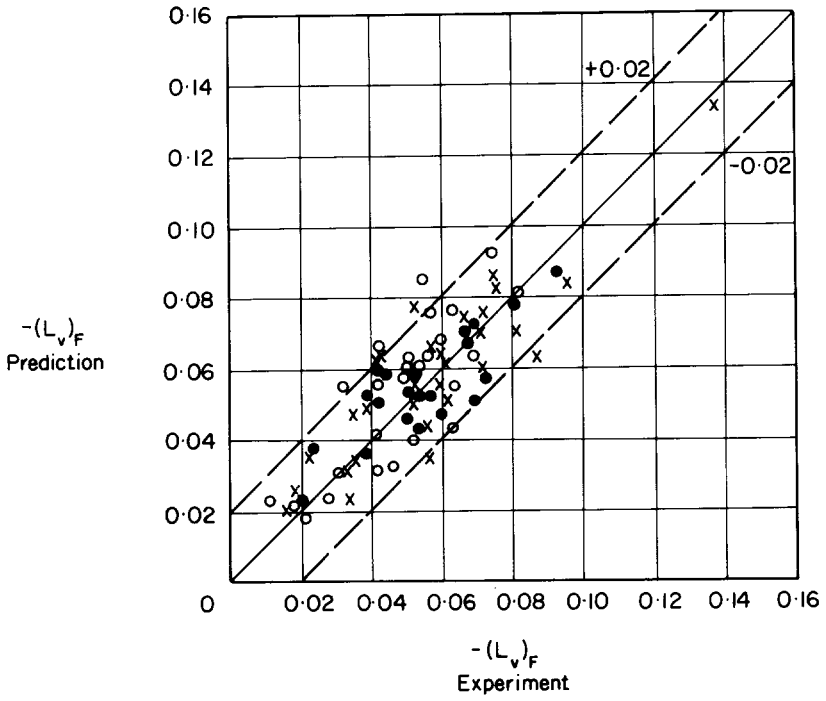

Sketch 4.3

4.2 Applicability

4.2.1 General

The method is applicable to conventional aircraft in the cruise (clean) configuration at small angles of attack and sideslip where there is an essentially linear variation of the sideforce, yawing moment and rolling moment with the angle of sideslip. In practice, because of departures from a linear variation, static lateral stability derivatives are defined from experimental data over a small range of sideslip angles about 0, typically between $\pm 2°$ or $\pm 5°$. The derivatives predicted by the method in this Item are consistent with this approach. The experimental data in Derivations 1 to 31 suggest that at angles of attack and lift coefficients representative of cruise conditions low-wing and mid-wing aircraft tend to maintain a linear variation of sideforce, yawing moment and rolling moment for sideslip angles approaching 10°. The data for high-wing aircraft often start to show some departure from a linear variation between 5° and 10° of sideslip, with the magnitudes of the sideforce, yawing moment and rolling moment slowly increasing.

Almost all of the data studied were from wind-tunnel tests carried out at low speeds and the method introduces compressibility effects only through the basic fin lift-curve slope estimated from Item No. 70011. However, a few experimental data (Derivations 15, 18, 22, 23 and 25) were available for configurations tested at Mach numbers of 0.6 and 0.8 and in these cases the stability derivatives were predicted with an accuracy comparable to that for the low-speed data. It is therefore suggested that the method can be used generally for subsonic free-stream Mach numbers, provided that the flow over the configuration is fully attached and wholly subsonic.

The range of configuration geometries considered is illustrated in Table 4.1, where the more important parameters are listed. The method should only be used with caution for configurations which depart significantly from these. In particular, the range of $h_{BF}/(h_{BF}+h_F)$ should be noted. For values of this parameter above 0.5 the body will become increasingly dominant and will alter the form of some of the correction factors. For values below 0.1 the fin will act increasingly as an isolated surface and the correction factors and centre of pressure position given assume the presence of a body with $h_{BF}/(h_{BF}+h_F) \geq 0.1$. It should also be noted that the method was developed for bodies of circular or nearly circular cross-section. Section 4.2.2 discusses the effect of different cross-sections.

The presence of jet-engine nacelles on the rear-body in the vicinity of the fin will cause some interference of the flow over the tail assembly and hence affect the stability derivatives. The magnitude of this effect will depend on the size and position of the nacelles involved and no general prediction method is attempted. In one particular case (from Derivation 30), for example, large nacelles mounted close to the fin caused an increase of –0.1 in $(Y_v)_F$ and +0.024 in $(N_v)_F$. The effect of rear nacelles on $(L_v)_F$ is usually small enough to be ignored.

TABLE 4.1 Range of Geometries

Body		*Wing*		*Fin*		*Tailplane**	
$h_{BF}/(h_{BF}+h_F)$	0.1 to 0.5	A_W	2 to 11	A_F	1.0 to 5.0	A_T	0.5 to 5.5
h_{BF}/d_{BF}	1 to 1.15	$\Lambda_{¼W}$	0° to 60°	$\Lambda_{¼F}$	0 to 60°	$\Lambda_{¼T}$	0 to 60°
		z_W/h_{BW}	0.5 to –0.5	λ_F	0 to 1	λ_T	0 to 1
				S_F/S_W	0.05 to 0.27	b_T/h_F	0.5 to 4

*The height of fin-mounted tailplanes is assumed to lie in the range $0.25 \leq z_T/h_F \leq 1$. The root chord of the tailplane is assumed to be of comparable magnitude to the local fin chord for fin-mounted tailplanes and to the fin root chord for body-mounted tailplanes.

4.2.2 Bodies of non-circular cross-section

An examination was made of the small number of experimental data (Derivations 2, 20, 23, 28, 29 and 31) available for bodies with irregular, elliptical or near-rectangular cross-section (including square). The results of this suggest that if a mean body diameter of $(h_{BF} + d_{BF})/2$ is substituted for h_{BF} throughout the method, then regardless of cross-sectional shape the stability derivatives for the fin are predicted with an overall accuracy comparable to that achieved for bodies of circular cross-section. This was found even where the elliptical cross-section had a value of $h_{BF}/d_{BF} = 1.7$ and the near-rectangular cross-section had values $h_{BF}/d_{BF} = 1.7$ and 0.6 (Derivations 2 and 20). However, in view of the small number of data available for comparisons, the method should be used with caution for such bodies and it should be remembered that the wing-body contribution to Y_v and N_v is strongly affected by the cross-sectional shape, as shown in Item No. 79006. It is therefore recommended that use of the method be confined to cases where $0.8 \leq h_{BF}/d_{BF} \leq 1.2$ and that Item No. 93007 be used otherwise because its underlying theory allows a variation with h_{BF}/d_{BF}.

4.2.3 Dorsal fin extensions

Many fins have a small dorsal fin extension at the bottom of the fin leading-edge which runs forward along the top of the body, as shown shaded in Sketch 3.1. These extensions are added to produce a vortex flow over the lower part of the fin which grows in strength as the sideslip angle increases and maintains the fin effectiveness at high angles of sideslip (above about 10°) where flow separation over the main part of the fin would otherwise result in a rapid loss of fin effectiveness. (See Reference 40, for example.) The dorsal fin has little effect on the lateral stability at low angles of sideslip where the associated vortex flow is weak, and the experimental data studied suggest that it can be ignored provided area is less than about $0.15 S_F$.

5. DERIVATION AND REFERENCES

5.1 Derivation

The Derivation lists selected sources of information that have assisted in the preparation of this Item.

Wind-tunnel Data

1. BAMBER, M.J.; HOUSE, R.O. — Wind-tunnel investigation of effect of yaw on lateral-stability characteristics. II – Rectangular NACA 23012 wings with a circular fuselage and a fin. NACA tech. Note 730, 1939.

2. HOUSE, R.O.; WALLACE, A.R. — Wind-tunnel investigation of effect of interference on lateral stability characteristics of four NACA 23012 wings, an elliptical and a circular fuselage and vertical fins. NACA Rep. 705, 1941.

3. RECANT, I.G. — Wind-tunnel investigation of effect of yaw on lateral-stability characteristics. III – Symmetrically tapered wing at various positions on circular fuselage with and without a vertical tail. NACA tech. Note 825, 1941.

4. WALLACE, A.R.; TURNER, T.R. — Wind-tunnel investigation of effect of yaw on lateral-stability characteristics. V – Symmetrically tapered wing with a circular fuselage having a horizontal and a vertical tail. NACA ARR 3F23 (TIL 456), 1943.

5. MURRAY, H.E. — Wind-tunnel investigation of end-plate effects of horizontal tails on a vertical tail compared with available theory. NACA tech. Note 1050, 1946.

6. BIRD, J.D. LICHTENSTEIN, J.H. JAQUET, B.M. — Investigation of the influence of fuselage and tail surfaces on low-speed static stability and rolling characteristics of a swept-wing model. NACA tech. Note 2741 1947.

7. BREWER, J.D. LICHTENSTEIN, J.H. — Effect of horizontal tail on low-speed static lateral stability characteristics of a model having 45° sweptback wing and tail surfaces. NACA tech. Note 2010, 1949.

8. KIRBY, D.A. — Low speed tunnel tests on a 1/5th scale model of a single-jet fighter with a 40° sweptback wing. RAE Rep. aero. 2382, 1950.

9. LETKO, W. RILEY, D.R. — Effect of an unswept wing on the contribution of unswept-tail configurations to the low-speed static- and rolling-stability derivatives of a midwing airplane model. NACA tech. Note 2175, 1950.

10. QUEIJO, M.J. WOLHART, W.D. — Experimental investigation of the effect of vertical-tail size and length and of fuselage shape and length on the static lateral stability characteristics of a model with 45° sweptback wing and tail surfaces. NACA Rep. 1049, 1951.

11. GOODMAN, A. — Effects of wing position and horizontal-tail position on the static stability characteristics of models with unswept and 45° sweptback surfaces with some reference to mutual interference. NACA tech. Note 2504, 1951.

12. QUEIJO, M.J. WELLS, E.G. — Wind-tunnel investigation of the low-speed static and rotary stability derivatives of a 0.13-scale model of the Douglas D-558-II airplane in the landing configuration. NACA RM L52G07 (TIL 3502), 1952.

13. LAWFORD, J.A. — A method of estimating the sideforce due to fins, based on a body-fin theory. RAE Rep. aero. 2493, 1953.

14. GOODMAN, A. THOMAS, D.F. — Effects of wing position and fuselage size on the low-speed static and rolling stability characteristics of a delta-wing model. NACA tech. Note 3063, 1953.

15. WILEY, H.G. RILEY, D.R. — An experimental and theoretical investigation at high subsonic speeds of the effects of horizontal-tail height on the aerodynamic characteristics in sideslip of an unswept, untapered tail assembly. NACA RM L53J19 (TIL 4034), 1953.

16. GRINER, R.F. — Static lateral stability characteristics of an airplane model having a 47.7° sweptback wing of aspect ratio 6 and the contribution of various model components at a Reynolds number of 4.45×10^6. NACA RM L53G09 (TIL 3885), 1953.

17. MICHAEL, W.H. — Investigation of mutual interference effects of several vertical-tail-fuselage configurations in sideslip. NACA tech. Note 3135, 1953.

18. WIGGINS, J.W.
KUHN, R.E.
FOURNIER, P.G.
Wind-tunnel investigation to determine the horizontal- and vertical-tail contributions to the static lateral stability characteristics of a complete-model swept-wing configuration at high subsonic speeds. NACA tech. Note 3818, 1953.

19. RILEY, D.R.
Effect of horizontal-tail span and vertical location on the aerodynamic characteristics of an unswept tail assembly in sideslip. NACA Rep. 1171, 1954.

20. LETKO, W.
WILLIAMS, J.L.
Experimental investigation at low speeds of effects of fuselage cross-section on static longitudinal and lateral stability characteristics of models having 0° and 45° sweptback surfaces. NACA tech. Note 3551, 1955.

21. WOLHART, W.D.
THOMAS, D.F.
Static longitudinal and lateral stability characteristics at low speed of unswept-mid-wing models having wings with aspect ratio of 2, 4 or 6. NACA tech. Note 3649, 1955.

22. FEW, A.G.
Investigation at high subsonic speeds of the static lateral and directional stability and tail-loads. Characteristics of a model having a highly tapered swept wing of aspect ratio 3 and two horizontal-tail positions. NACA RM L56E29 (TIL 5217), 1956.

23. HALLISSY, J.M.
Transonic wind-tunnel measurements of static lateral and directional stability and vertical-tail loads for a model with a 45° sweptback wing. NACA RM L55L19 (TIL 6683), 1956.

24. SILVERS, N.H.
KING, T.J.
Investigation at high subsonic speeds of the effect of horizontal-tail location on longitudinal and lateral stability characteristics of a complete model having a sweptback wing in a high location. NACA RM 58B10 (TIL 5071), 1956.

25. SLEEMAN, W.C.
An experimental study at high subsonic speeds of several tail configurations on a model having a 45° sweptback wing. NACA RM L57C08 (TIL 5495), 1957.

26. THOMAS, D.F.
WOLHART, W.D.
Static longitudinal and lateral stability characteristics at low speed of 45° sweptback – midwing models having wings with an aspect ratio of 2, 4 or 6. NACA tech. Note 4077, 1957.

27. WOLHART, W.D.
THOMAS, D.F.
Static longitudinal and lateral stability characteristics at low speed of 60° sweptback – midwing models having wings with an aspect ratio of 2, 4 or 6. NACA tech. Note 4397, 1958.

28. CHAMBERS, J.R.
ANGLIN, E.L.
Analysis of lateral directional – stability characteristics of a twin-jet fighter airplane at high angles of attack. NASA tech. Note D-5361, 1969.

29. MARGASON, R.J.
VOGLER, R.D.
Wind-tunnel investigation at low speeds of a model of the Kestrel (XV-6A) vectored-thrust V/STOL airplane. NASA tech. Note D-6826, 1972.

30. BAe
Unpublished wind-tunnel data from British Aerospace, Aircraft Group, Hatfield-Chester, Warton and Weybridge-Bristol Divisions.

31. SAAB-SCANIA
Unpublished wind-tunnel data from Saab-Scania, Sweden.

Theoretical Data

32. WEBER, J.
HAWK, A.C. Theoretical load distributions on fin-body-tailplane arrangements in a side-wind. ARC R & M 2992, 1957.

ESDU Items

33. ESDU Lift-curve slope and aerodynamic centre position of wings in inviscid subsonic flow. Item No. 70011, Engineering Sciences Data Unit, London, July 1970.

5.2 References

The References list selected sources of information supplementary to that given in this Item.

ESDU Items

34. ESDU Lift-curve slope for single fin and rudder. (i) Body shape merging into fin. Item No. Aero C.01.01.01, Engineering Sciences Data Unit, London, January 1955.

35. ESDU Stability derivative $(L_v)_\Gamma$. Contribution of full-span dihedral to rolling moment due to sideslip, Item No. Aero A.06.01.03, Engineering Sciences Data Unit, London, April 1955.

36. ESDU Wing-body yawing moment and sideforce derivatives due to sideslip: N_v and Y_v. Item No. 79006, Engineering Sciences Data Unit, London, June 1979.

37. ESDU Estimation of rolling moment derivative due to sideslip for complete aircraft at subsonic speeds. Item No. 81032, Engineering Sciences Data Unit, London, October 1981.

38. ESDU Estimation of sideforce and yawing moment derivatives due to sideslip for complete aircraft at subsonic speeds. Item No. 82011, Engineering Sciences Data Unit, London, September 1982.

39. ESDU Contribution of body-mounted fins and tailplanes to lateral derivatives due to sideslip at subsonic speeds for general body width to height ratio. ESDU International, Item No. 93007, 1993.

40. DAVIDSON, P. Directional stability and control of the Cranfield A1. CIT Cranfield MSc Thesis, September 1980.

6. EXAMPLE

Calculate the fin component of the static lateral stability derivatives for the wing-body configuration shown in Sketch 6.1 with each of the three fin-tailplane arrangements shown in Sketch 6.2. The fin and tailplane planforms are unaltered as the tailplane position varies.

A Mach number of 0.8 and an angle of attack of 2° may be assumed. The stability derivatives should be based on a reference area S_W = 320 m^2 and a span b = 45.0 m.

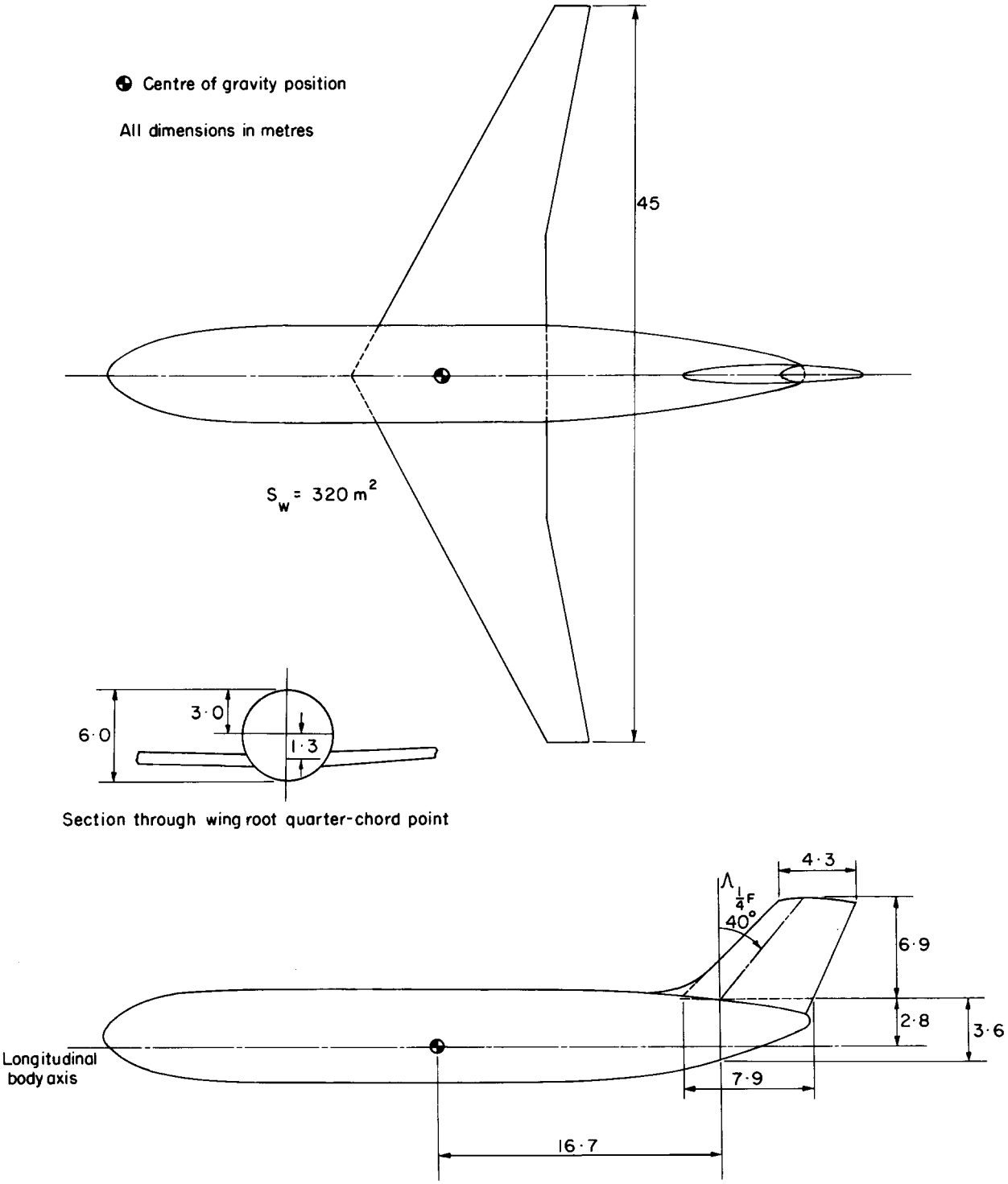

Sketch 6.1

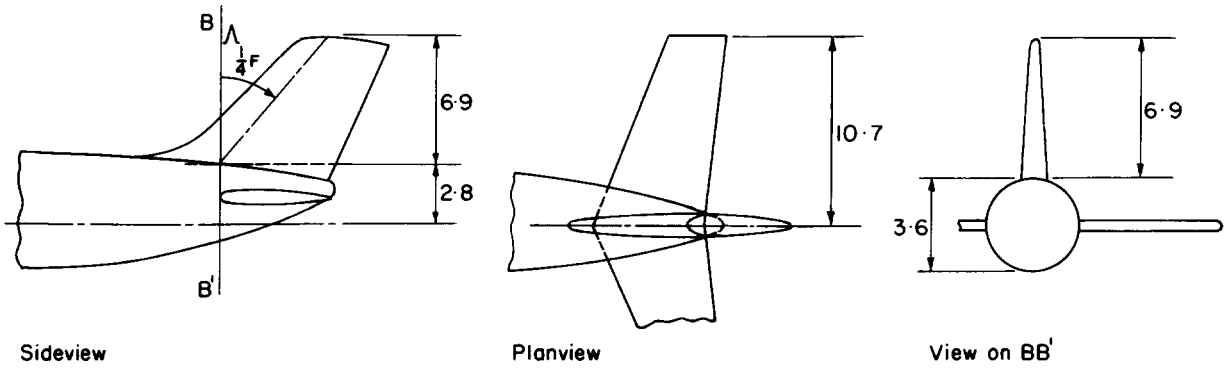

Sideview | Planview | View on BB'

a. Tailplane mounted on body

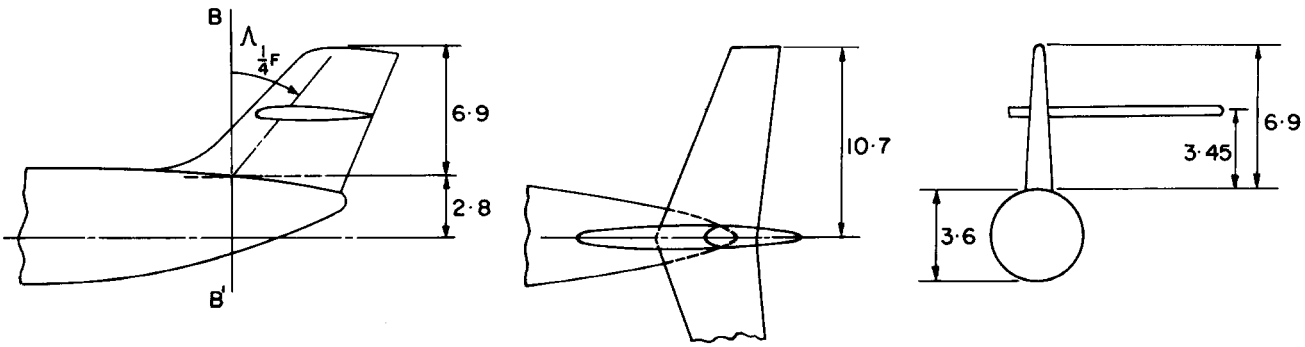

Sideview | Planview | View on BB'

b. Tailplane mounted at mid-fin

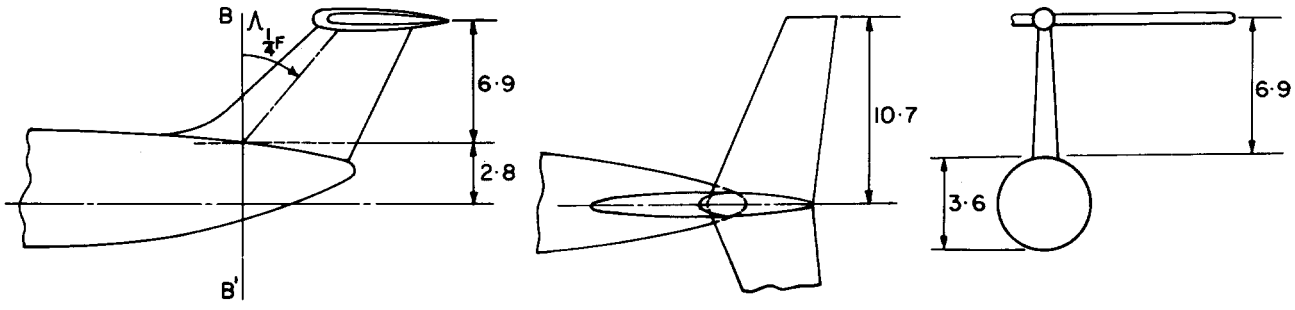

Sideview | Planview | View on BB'

c. Tailplane mounted at top of fin

Sketch 6.2

6.1 Calculate $(C_{L\alpha})_F$

The basic lift-curve slope of the fin is calculated as described in Section 3.2. The area of the basic trapezium, using the dimensions in Sketch 6.1, is given by Equation (3.5)

$$S_F = h_F(c_{rF} + c_{tF})/2$$
$$= 6.9\ (7.9 + 4.3)/2 = 42.1\ \text{m}^2\ .$$

Using Equations (3.6) to (3.8), the straight-tapered wing produced by reflecting the trapezium about its root chord has an aspect ratio

$$A_F = 2h_F^2\ /S_F$$
$$= 2 \times 6.9^2/42.1 = 2.26\ ,$$

a taper ratio

$$\lambda_F = c_{tF}\ /c_{rF}$$
$$= 4.3/7.9 = 0.54\ ,$$

and a half-chord sweep angle parameter defined by the equation

$$A_F \tan\Lambda_{½F} = A_F \tan\Lambda_{¼F} - \left(\frac{1-\lambda_F}{1+\lambda_F}\right)$$
$$= 2.26 \tan 40° - \frac{1-0.54}{1+0.54} = 1.60\ .$$

For a Mach number of 0.8, $(1-M^2)^{½}\ A_F = (1-0.8^2)^{½} \times 2.26 = 1.36.$

Using the values calculated for $(1-M^2)^{½}\ A_F$, $A_F \tan\Lambda_{½F}$ and λ_F, Item No. 70011 gives

$$(C_{L\alpha})_F\ /A_F = 1.33\ ,$$

so $$(C_{L\alpha})_F = 1.33 \times 2.26 = 3.01 \text{ per radian.}$$

6.2 Calculation of J_B, J_T and J_W

(i) For all three tailplane positions

$$A_F = 2.26\ ,$$

and $$h_{BF}\ /(h_{BF} + h_F) = 3.6/(3.6 + 6.9) = 0.343\ .$$

Therefore, from Figure 1 $J_B = 1.13$ in each case.

(ii) For the body-mounted tailplane

$$h_{BF}/(h_{BF}+h_F) = 0.343$$

and $$b_T/h_F = 2 \times 10.7/6.9 = 3.10\,.$$

Therefore, from Figure 2a $J_T = 1.12$.

For the tailplane mounted at the mid-fin position

$$b_T/h_F = 3.10$$

and $$(z_T/h_F)^2 = (3.45/6.9)^2 = 0.25\,.$$

Therefore, from Figure 2b $J_T = 0.98$.

For the tailplane mounted at the top of the fin

$$b_T/h_F = 3.10$$

and $$(z_T/h_F)^2 = 1.0\,.$$

Therefore, from Figure 2b $J_T = 1.30$.

(iii) From the wing-body geometry

$$z_W/h_{BW} = 1.3/6.0 = 0.22.$$

Therefore, for the body-mounted tailplane, Figure 3a gives $J_W = 1.07$ and for the two fin-mounted tail-planes, Figure 3b gives $J_W = 1.13$.

6.3 Calculation of $(Y_v)_F$

Substitution in Equation (3.1) of the basic fin lift-curve slope from Section 6.1 and the correction factors from Section 6.2 gives

$$(Y_v)_F = -J_B J_T J_W (C_{L\alpha})_F S_F/S_W$$
$$= -1.13 \times 1.12 \times 1.07 \times 3.01 \times 42.1/320$$
$$= -0.54 \text{ for the tailplane mounted on the body,}$$

$$(Y_v)_F = -1.13 \times 0.98 \times 1.13 \times 3.01 \times 42.1/320$$
$$= -0.50 \text{ for the tailplane mounted at the mid-fin position, and}$$

$$(Y_v)_F = -1.13 \times 1.30 \times 1.13 \times 3.01 \times 42.1/320$$
$$= -0.65 \text{ for the tailplane mounted at the top of the fin.}$$

6.4 Calculation of Centre of Pressure Position

The centre of pressure position is determined as described in Section 3.6.

For the body-mounted tailplane, Figure 4 gives $\bar{z}_F / h_F = 0.4$.

For the tailplane mounted at the mid-fin position $z_T / h_F = 0.5$ and Figure 4 gives $\bar{z}_F / h_F = 0.473$. For the tailplane mounted at the top of the fin $z_T / h_F = 1$ and Figure 4 gives $\bar{z}_F / h_F = 0.6$.

From Sketch 6.1, $m_F = 16.7$ m, $z_{crF} = 2.8$ m and $\Lambda_{¼F} = 40°$. Therefore the moment arms of the sideforce in directions perpendicular and parallel to the longitudinal body axis are, from Section 3.6,

$$z_{crF} + 0.85\bar{z}_F = 2.8 + 0.85 \times 0.4 \times 6.9 = 5.15 \text{ m}$$

and $$m_F + 0.7\bar{z}_F \tan\Lambda_{¼F} = 16.7 + 0.7 \times 0.4 \times 6.9 \times \tan 40° = 18.32 \text{ m}$$

for the body-mounted tailplane,

$$z_{crF} + 0.85\bar{z}_F = 2.8 + 0.85 \times 0.473 \times 6.9 = 5.57 \text{ m}$$

and $$m_F + 0.7\bar{z}_F \tan\Lambda_{¼F} = 16.7 + 0.7 \times 0.473 \times 6.9 \times \tan 40° = 18.62 \text{ m}$$

for the tailplane mounted at the mid-fin position, and

$$z_{crF} + 0.85\bar{z}_F = 2.8 + 0.85 \times 0.6 \times 6.9 = 6.32 \text{ m}$$

and $$m_F + 0.7\bar{z}_F \tan\Lambda_{¼F} = 16.7 + 0.7 \times 0.6 \times 6.9 \times \tan 40° = 19.13 \text{ m}$$

for the tailplane mounted at the top of the fin.

6.5 Calculation of $(N_v)_F$ and $(L_v)_F$

The values of $(N_v)_F$ and $(L_v)_F$ are obtained by substituting the sideforce derivative from Section 6.3, the moment arms from Section 6.4, and an angle of attack of 2° in Equations (3.2) and (3.3),

$$(N_v)_F = -(Y_v)_F [(m_F + 0.7\bar{z}_F \tan\Lambda_{¼F})\cos\alpha + (z_{crF} + 0.85\bar{z}_F)\sin\alpha]/b$$

and $$(L_v)_F = (Y_v)_F [(z_{crF} + 0.85\bar{z}_F)\cos\alpha - (m_F + 0.7\bar{z}_F \tan\Lambda_{¼F})\sin\alpha]/b .$$

Thus,

$$(N_v)_F = 0.54[18.32\cos 2° + 5.15\sin 2°]/45.0 = 0.22$$

and $$(L_v)_F = -0.54[5.15\cos 2° - 18.32\sin 2°]/45.0 = -0.054$$

for the body-mounted tailplane,

$$(N_v)_F = 0.50[18.62\cos 2° + 5.57\sin 2°]/45.0 = 0.21$$

and $$(L_v)_F = -0.50[5.57\cos 2° - 18.62\sin 2°]/45.0 = -0.055$$

for the tailplane at the mid-fin position, and

$$(N_v)_F = 0.66[19.13\cos 2° + 6.32\sin 2°]/45.0 = 0.28$$

and $$(L_v)_F = -0.66[6.32\cos 2° - 19.13\sin 2°]/45.0 = -0.083$$

for the tailplane at the top of the fin.

6.6 Summary

The values of the lateral stability derivatives for the three tail arrangements are summarised in Table 6.1.

TABLE 6.1

$(Y_v)_F$	$(N_v)_F$	$(L_v)_F$	*Configuration*
– 0.54	0.22	– 0.054	Tailplane mounted on body
– 0.50	0.21	– 0.055	Tailplane mounted at mid-fin position
– 0.66	0.28	– 0.083	Tailplane mounted at top of fin

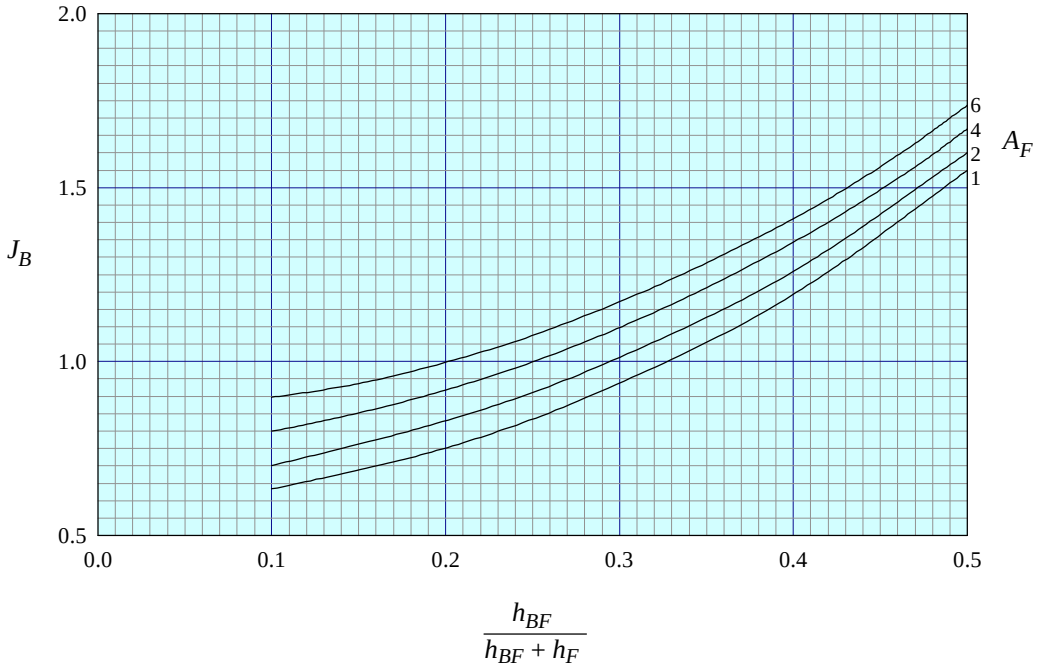

FIGURE 1 BODY-FIN CORRECTION FACTOR

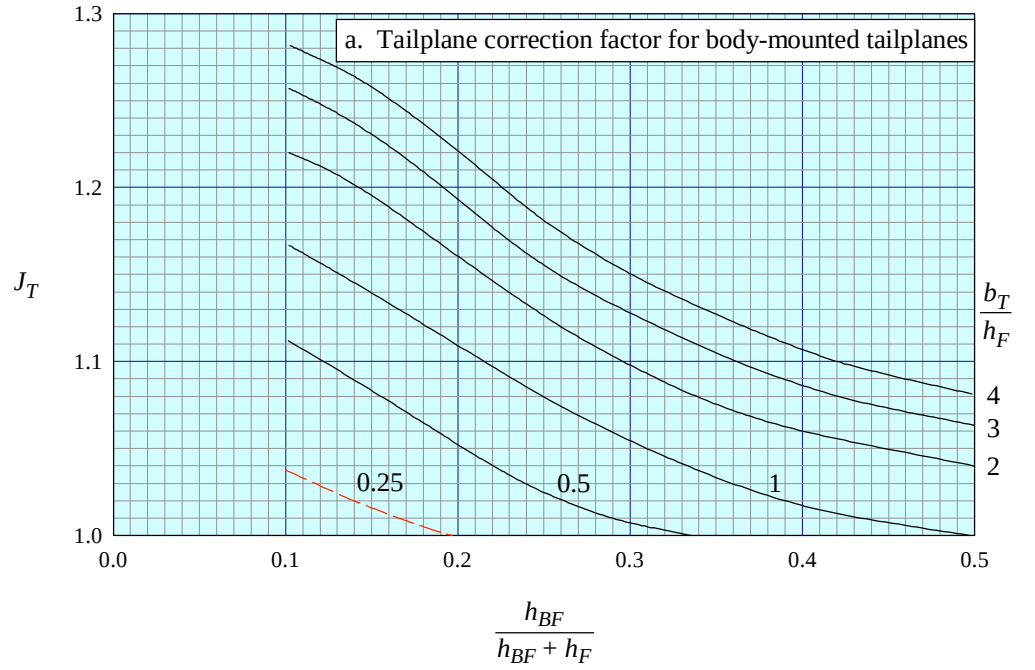

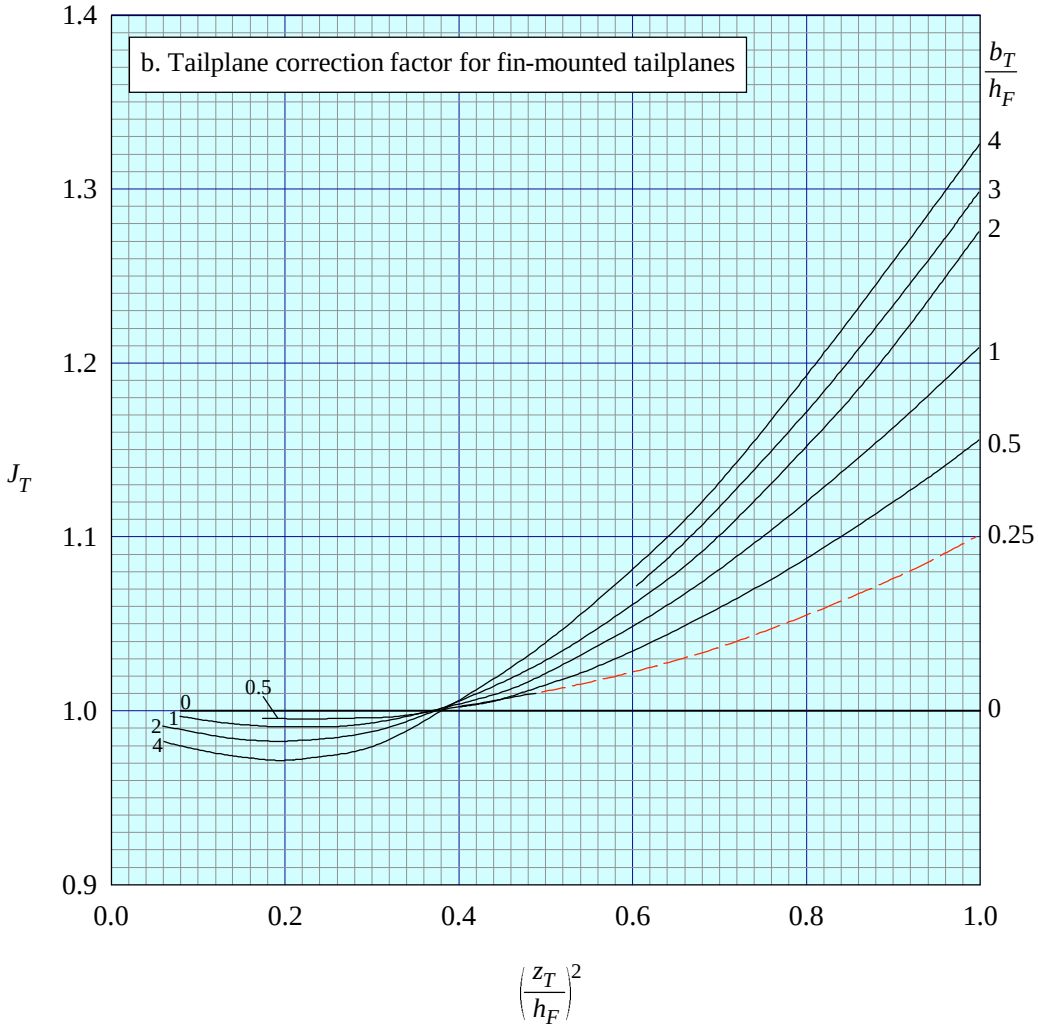

FIGURE 2 TAILPLANE CORRECTION FACTOR

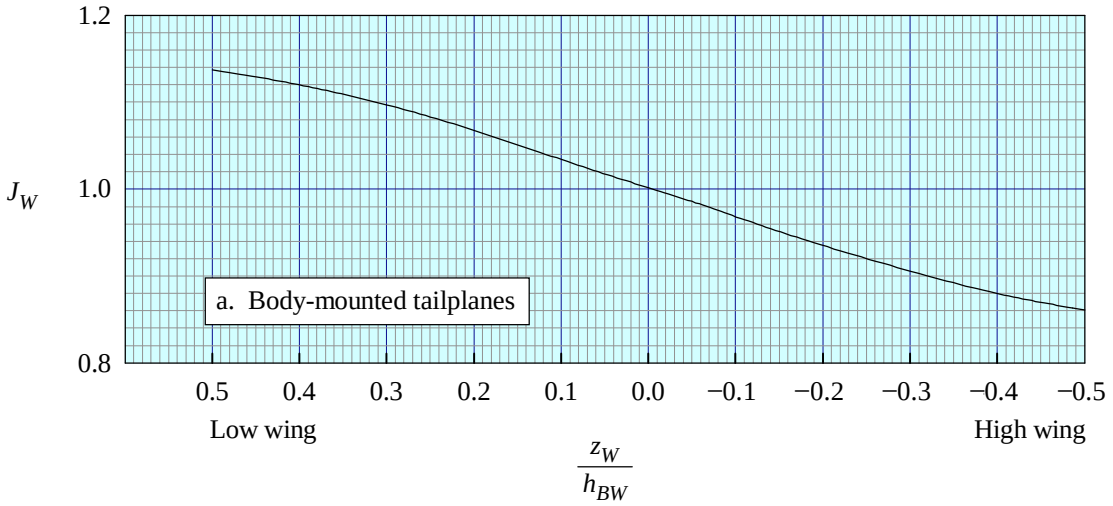

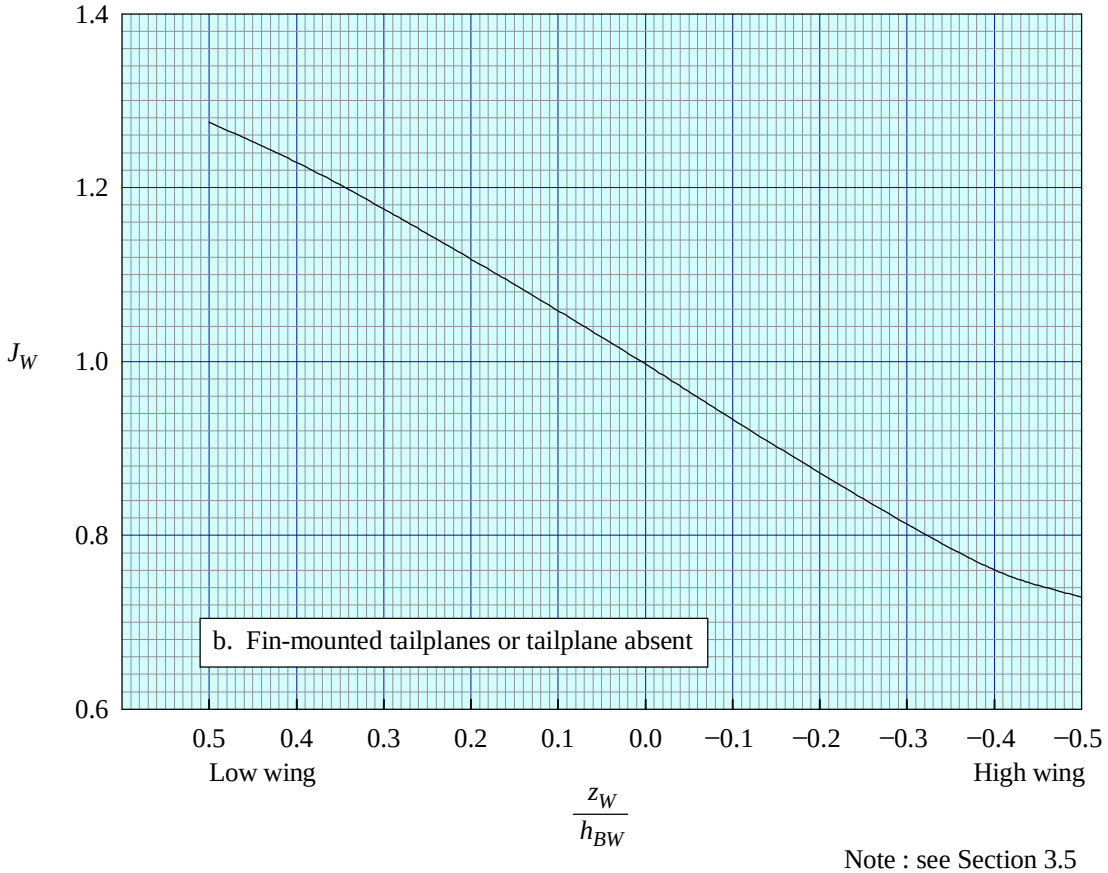

Note : see Section 3.5

FIGURE 3 WING CORRECTION FACTOR

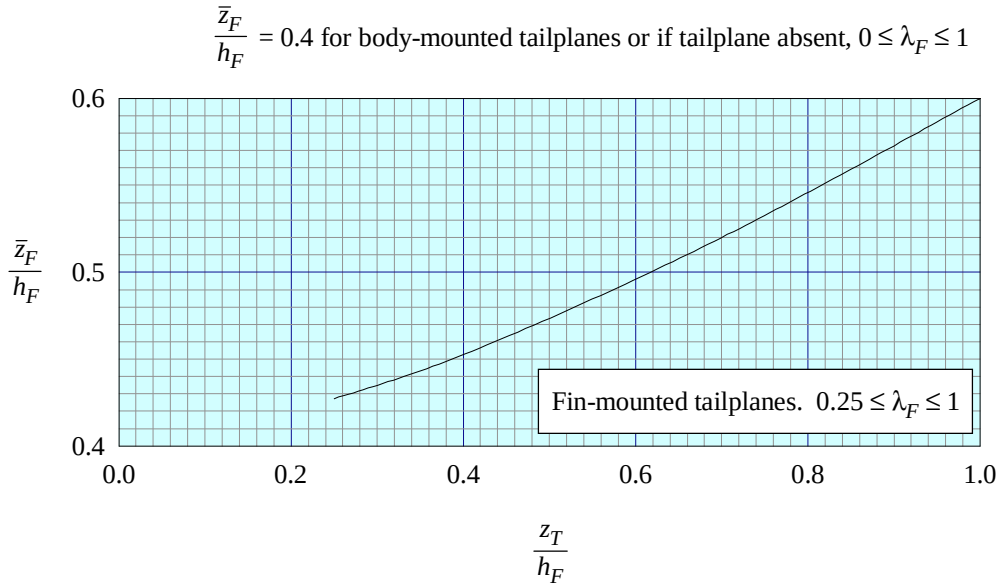

FIGURE 4 HEIGHT OF CENTRE OF PRESSURE POSITION OF LOAD DISTRIBUTION ON FIN

THE PREPARATION OF THIS DATA ITEM

The work on this particular Item, which supersedes Item No. Aero. C.01.01.05 and, in part, Item No. 70006, was monitored and guided by the Aerodynamics Committee which first met in 1942 and now has the following membership:

Chairman

Mr P.K. Jones	–	British Aerospace, Manchester Division

Vice-Chairman

Mr J. Weir	–	Salford University

Members

Mr D. Bonenfant	–	Aérospatiale, Toulouse, France
Mr E.A. Boyd	–	Cranfield Institute of Technology
Mr K. Burgin	–	Southampton University
Mr E.C. Carter	–	Aircraft Research Association
Mr J.R.J. Dovey	–	British Aerospace, Warton Division
Dr J.W. Flower	–	Bristol University
Mr H.C. Garner	–	Royal Aircraft Establishment
Mr A. Hipp	–	British Aerospace, Stevenage-Bristol Division
Dr B.L. Hunt*	–	Northrop Corporation, Hawthorne, Calif., USA
Mr J. Kloos*	–	Saab-Scania, Linköping, Sweden
Mr J.R.C. Pedersen	–	Independent
Mr I.H. Rettie*	–	Boeing Aerospace Company, Seattle, Wash., USA
Mr F.W. Stanhope	–	Rolls-Royce Ltd, Derby
Mr H. Vogel	–	British Aerospace, Weybridge-Bristol Division.

* Corresponding Member

The member of staff who undertook the technical work involved in the initial assessment of the available information and the construction and subsequent development of the Item was

Mr R.W. Gilbey	–	Senior Engineer.